Inverse Optical Torques on Dielectric Nanoparticles in Elliptically Polarized Light Waves

Yuzhi Shi,[1,2,3,4,*] Tongtong Zhu,[5] Ai Qun Liu,[6,†] Lei-Ming Zhou,[7,8] Manuel Nieto-Vesperinas,[9] Amir Hassanfiroozi,[10] Jingquan Liu,[11] Din Ping Tsai,[12] Zhenyu Li,[6] Weiqiang Ding,[13] Fan Wang,[14] Hang Li,[8,13] Qinghua Song,[15] Xiaohao Xu,[16] Baojun Li,[16] Xinbin Cheng,[1,2,3,4] Pin Chieh Wu,[10] Che Ting Chan,[17] and Cheng-Wei Qiu[8,‡]

[1]*Institute of Precision Optical Engineering, School of Physics Science and Engineering, Tongji University, Shanghai 200092, China*
[2]*MOE Key Laboratory of Advanced Micro-Structured Materials, Shanghai 200092, China*
[3]*Shanghai Institute of Intelligent Science and Technology, Tongji University, Shanghai 200092, China*
[4]*Shanghai Frontiers Science Center of Digital Optics, Shanghai 200092, China*
[5]*School of Optoelectronic Engineering and Instrumentation Science, Dalian University of Technology, Dalian 116024, China*
[6]*School of Electrical and Electronic Engineering, Nanyang Technological University, Singapore 639798, Singapore*
[7]*Department of Optical Engineering, School of Physics, Hefei University of Technology, Hefei 230601, China*
[8]*Department of Electrical and Computer Engineering, National University of Singapore, Singapore 117583, Singapore*
[9]*Instituto de Ciencia de Materiales de Madrid, Consejo Superior de Investigaciones Científicas, Campus de Cantoblanco, Madrid 28049, Spain*
[10]*Department of Photonics, National Cheng Kung University, Tainan 70101, Taiwan*
[11]*National Key Laboratory of Science and Technology on Micro/Nano Fabrication, Shanghai Jiao Tong University, Shanghai 200240, China*
[12]*Department of Electrical Engineering, City University of Hong Kong, Hong Kong, China*
[13]*School of Physics, Harbin Institute of Technology, Harbin 150001, China*
[14]*School of Physics, Beihang University, Beijing 100191, China*
[15]*Tsinghua Shenzhen International Graduate School, Tsinghua University, Shenzhen 518055, China*
[16]*Institute of Nanophotonics, Jinan University, Guangzhou 511443, China*
[17]*Department of Physics, The Hong Kong University of Science and Technology, Hong Kong, China*

(Received 11 October 2021; accepted 29 June 2022; published 28 July 2022)

Elliptically polarized light waves carry the spin angular momentum (SAM), so they can exert optical torques on nanoparticles. Usually, the rotation follows the same direction as the SAM due to momentum conservation. It is counterintuitive to observe the reversal of optical torque acting on an ordinary dielectric nanoparticle illuminated by an elliptically or circularly polarized light wave. Here, we demonstrate that negative optical torques, which are opposite to the direction of SAM, can ubiquitously emerge when elliptically polarized light waves are impinged on dielectric nanoparticles obliquely. Intriguingly, the rotation can be switched between clockwise and counterclockwise directions by controlling the incident angle of light. Our study suggests a new playground to harness polarization-dependent optical force and torque for advancing optical manipulations.

DOI: 10.1103/PhysRevLett.129.053902

Optical forces and torques have been widely utilized to manipulate micro- and nanoscale objects for pushing [1–3], pulling [4–7], lateral deflecting [8–10], and trapping [11,12]. Polarization-anisotropic particles (e.g., rod or dumbbell) can be aligned along the polarization direction of light by the conservative optical torque [13] in a linearly polarized beam. They can also experience optical torques from gradient forces in noncircular laser spots [14].

Circularly polarized light waves carrying angular momenta rotate nonspherical particles with nonconservative optical torques in the same direction as the spin angular momentum (SAM) **s**, being known as the "positive optical torque" (POT) [15–20], which can originate from the optical scattering and absorption [20,21]. The imaginary Poynting momentum density of cylindrical vector beams, with zero global spin and orbital angular momenta, induces a local nonzero angular momentum capable of rotating isotropic spheres [22]. The opposite, "negative optical torque" (NOT), was found in the "windmill effect" [20,23,24] as a consequence of radiation pressure being projected into the lateral direction due to the slant surface. It could also be found on complex micromachines [25] analogous to the windmill effect. Meanwhile, NOTs emerge on dipolar bianisotropic particles [16] and particle clusters illuminated by circularly polarized beams via the field retardation [26,27] and many-body interactions [28]. The NOT, also known as "left-handed torque," can exist in a single phase-retardation plate [29]. A wedge-shaped particle was reported to experience a NOT in a reverse direction with respect to the orbital angular momentum of the optical vortex [30], principally resembling the mechanism of optical pulling [31] and lateral forces

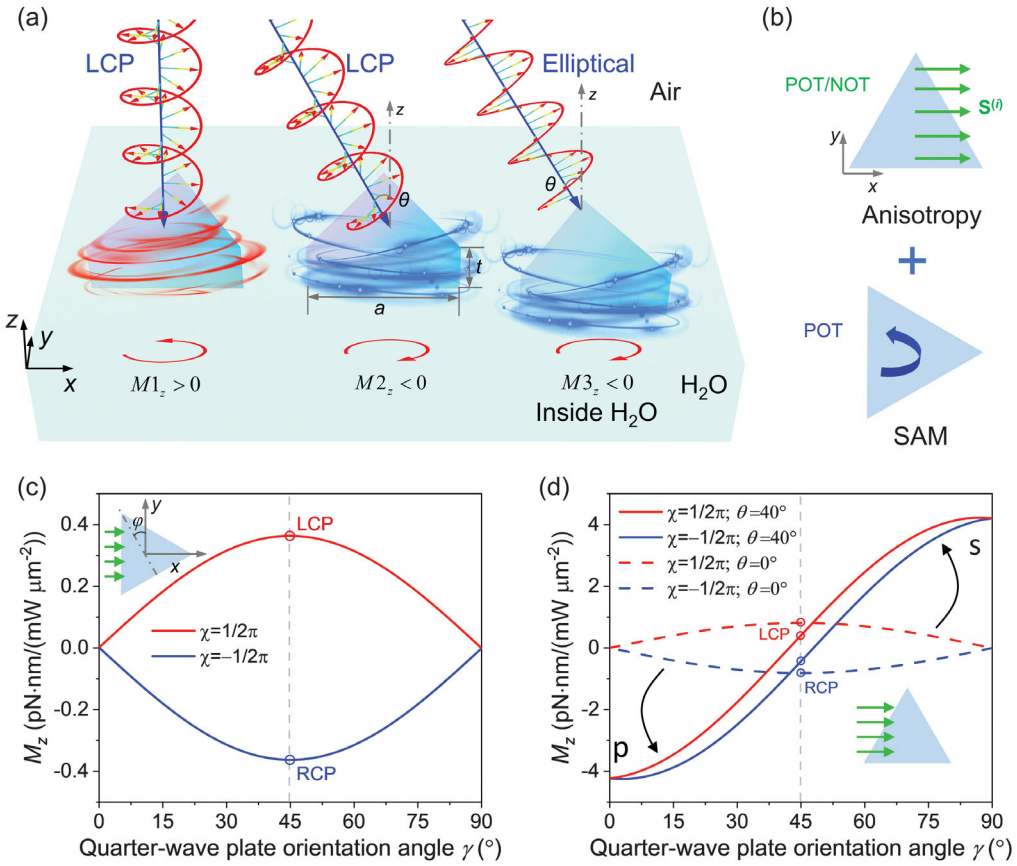

FIG. 1. Positive and negative optical torques on dielectric triangular prisms. (a) Schematics of the triangular prism (refractive index $n + ik$) placed at the interface of air ($n = 1$) and water ($n = 1.337$) and under the illumination of obliquely incident light beam (wavelength 532 nm, incident angle θ) with the left-handed circular polarization (LCP). The prism (side a, thickness t) rotates counterclockwise [top view, defined as the POT ($M_z > 0$)] when the incident angle $\theta = 0$. The NOT can emerge when the triangular prism is placed at the interface for the LCP, or immersed inside water for the elliptical polarization. (b) Schematics of the contributions from the geometric anisotropy and the SAM. $\mathbf{S}^{(i)}$ represents the incident Poynting vector. (c) Optical torque versus the orientation angle of the quarter-wave plate γ when the rotation angle of the triangular prism $\varphi = 30°$. Red and blue curves denote the ellipticity angles $\chi = 1/2\pi$ (phase delay in the y direction) and $\chi = -1/2\pi$, respectively. In this case with the geometry symmetry, $\mathbf{M}_{\text{aniso}} = 0$, and $\mathbf{M} = \mathbf{M}_{\text{SAM}}$. (d) Optical torque versus the orientation angle of the quarter-wave plate γ when $\varphi = 0$. When the incident angle $\theta = 40°$, $\mathbf{M}_{\text{aniso}} \neq 0$. The s and p polarizations correspond to the maximum POT and NOT, respectively. $\mathbf{M}_{\text{aniso}} = 0$, and $\mathbf{M} = \mathbf{M}_{\text{SAM}}$ when $\theta = 0$. In (c) and (d), $a = 150$ nm, $t = 150$ nm, and $\varepsilon_p = 16$.

[8,32]. The linearly polarized beam can excite two distinct plasmonic modes to generate both POT and NOT on a metallic chiral plasmonic nanostructure by the coupling of light and chirality [33]. Gain (negative imaginary part of refractive index) particles were found to experience reversible optical torques in linearly polarized beams [34]. By exciting high-order multipolar modes in plasmonic resonators, the NOT can be induced by the resonant scattering [35]. Despite extensive studies, in a general case, it is counterintuitive to envision a NOT in the opposite direction of $\mathbf{s}$ emerging on a dielectric nanoparticle illuminated by a single circularly polarized beam, as widely accepted by conventional dipole-mode theories [18,19].

Here, we unveil NOTs on an ordinary dielectric nonspherical nanoparticle controlled by different helicities of elliptically polarized light waves, that is, by different orientation angles of the quarter-wave plate. S and p polarizations, which induce the off-plane and in-plane dipole moments on a triangular prism, respectively, generate distinct distributions of optical forces, and thus opposite optical torques. The rotation directions of particles can also be easily switched between clockwise and counterclockwise using different incident angles of light with specific helicities. Our studies disclose the ubiquitous but long-neglected NOT, and provide new possibilities to harness reversible optical torques for various physical and biochemical applications.

To investigate the ubiquitous optical torques by an elliptically polarized beam, we consider a simple system: an equilateral triangular prism (refractive index, $n + ik$, $k = 0$) with side a and thickness t placed at a flat interface of air ($n_{\text{air}} = 1$) and water ($n_{\text{water}} = 1.337$), illuminated by

an obliquely incident circularly polarized light (wavelength, $\lambda = 532$ nm; incident angle, θ), as shown in Fig. 1(a). The strategy of utilizing the buoyancy at the interface serves as a paradigm for the investigation of intriguing optical phenomena and facilitates practical applications [8,31–33,36,37]. The prism rotates following the direction of the SAM when the beam is at normal incidence. For instance, it rotates counterclockwise (POT, top view) for the left-handed circular polarization (LCP). The optical torque on an electric dipole can be given under the dipole approximation as (see Supplemental Material [38]) [18,19,39]

$$\mathbf{M} = 8\pi\omega \mathrm{Im}(\alpha_e)\mathbf{s}_e, \qquad \alpha_e \approx \frac{\alpha_e^{(0)}}{1 - i\frac{2k^3}{3\varepsilon}\alpha_e^{(0)}}, \tag{1}$$

where $\mathbf{s}_e$ is the electric SAM, α_e is the electric polarizability with $\alpha_e^{(0)} = \varepsilon a^3[(\varepsilon_p - \varepsilon)/(\varepsilon_p + 2\varepsilon)]$, a is the radius of the particle, ε_p and ε are the permitivities of the particle and medium, respectively. $\mathrm{Im}(\alpha_e)$ is normally positive for an ordinary dielectric particle either with or without absorption (see Supplemental Material [38]). Taking a nonabsorbing dipole as an example, $\alpha_e^{(0)}$ is real, and $\mathrm{Im}(\alpha_e) > 0$, meaning that the optical torque (POT) is in the same direction as $\mathbf{s}_e$. The NOT can emerge on the triangular prism at the interface for the LCP, or immersed inside water for the elliptical polarization. The rigorous calculation of the optical torque on an arbitrarily sized and shaped particle, as adopted in this Letter, can be given as

$$\mathbf{M} = \oint_S (\mathbf{r} \times \overleftrightarrow{\mathbf{T}}) \cdot \hat{\mathbf{n}}\, dS, \tag{2}$$

where $\overleftrightarrow{\mathbf{T}}$ is the time-averaged Minkowski stress tensor [12], and S is a closed surface where we do the integral.

Though the optical torque is too complicated to be mathematically formulated for a nonspherical particle [40], we can interpret the torque by dividing it into terms from the geometric anisotropy and spin angular momentum (SAM) as $\mathbf{M} = \mathbf{M}_{\mathrm{aniso}} + \mathbf{M}_{\mathrm{SAM}}$ [Fig. 1(b)]. $\mathbf{M}_{\mathrm{aniso}}$, which can be positive and negative, originates from the scattering light by the geometry anisotropy, and can be obtained by subtracting the contribution from the SAM. Whereas $\mathbf{M}_{\mathrm{SAM}}$ is always positive, following the direction of $\mathbf{s}_e$. The simulation of optical torque (M_z) with the contribution only from the SAM can be visualized by rotating the prism ($\varepsilon_p = 16$) with $\varphi = 30°$, as shown in Fig. 1(c). M_z coincides with the amplitude and direction of the SAM (POT) as the quarter-wave plate orientation angle γ varies, and reaches the maximum values at the left-handed and right-handed circular polarizations (RCP). When the geometry anisotropy is deployed, e.g., $\varphi = 0$, the $\mathbf{M}_{\mathrm{aniso}}$ emerges with a strong correlation with γ, as shown in Fig. 1(d). The optical torque, when $\theta = 0$ (normal incidence and with $\mathbf{M}_{\mathrm{aniso}} = 0$), is very similar to Fig. 1(c). Whereas the small γ (approaching the p polarization) corresponds to a large NOT. In contrast, the large γ (approaching the s polarization) corresponds to a large POT. Therefore, we can conclude that the in-plane polarization (p polarization) is the dominating factor that surpasses the off-plane polarization (s polarization) and SAM to generate a NOT. This effect can be interpreted as the following: s and p polarizations polarize particles with dipole moments in different directions. The off-plane dipole moments by the s polarization and in-plane dipole moments by the p polarization, generate distinct distributions of optical forces, which induces opposite optical torques. Thus, the NOT strongly depends on the rotation of the triangular prism.

The high permittivity (e.g., $\varepsilon_p = 16$) is not essential to generate a NOT, as shown in Fig. 2(a), which plots the

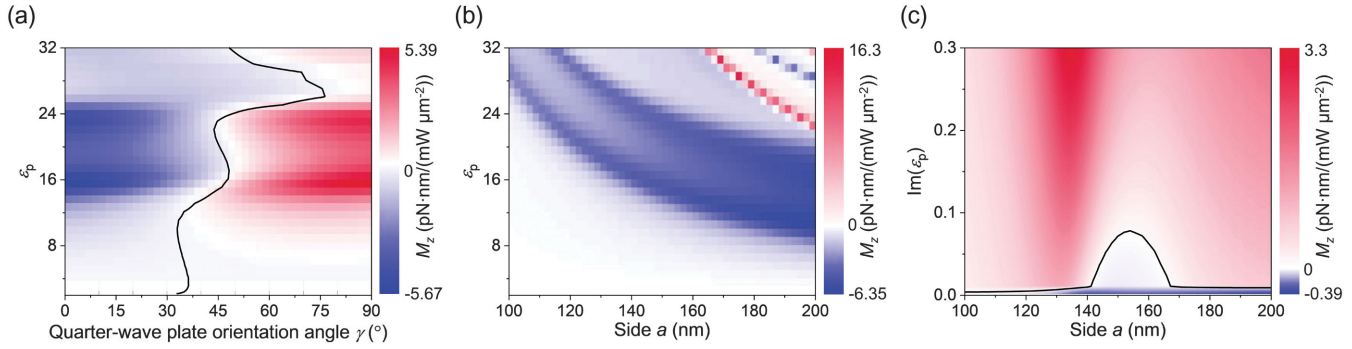

FIG. 2. Size-, permittivity-, and absorption-dependent NOTs. (a) Optical torque versus the orientation angle of the quarter-wave plate γ and the permittivity of particle ε_p. The small γ (approaching the p polarization) leads to the NOT, while the large γ (approaching the s polarization) leads to the POT. $\varepsilon_p > 15$ is required to obtain the NOT for the LCP ($\gamma = 45°$). $a = 150$ nm, $t = 150$ nm, and $\theta = 40°$. (b) Optical torque versus the side a and the permittivity ε_p of the particle. Most of M_z remain negative, while the POTs occur in the fringe with the high permittivity. $\gamma = 15°$, $t = 150$ nm, and $\theta = 40°$. (c) Influence of $\mathrm{Im}(\varepsilon_p)$ to the NOT. The presence of absorption significantly diminishes the NOT by introducing a POT from the absorption. $t = 150$ nm, $\mathrm{Re}(\varepsilon_p) = 16$, and $\theta = 40°$. In (a)–(c), the rotation angle of the triangular prism φ is 0. The contours in (a) and (c) denote $M_z = 0$.

optical torque versus ε_p and γ. The NOT can occur even for a low permittivity (e.g., $\varepsilon_p < 3$) when $\gamma < 30°$. For the LCP ($\gamma = 45°$), a high permittivity, i.e., $\varepsilon_p > 15$, is required to obtain the NOT. Meanwhile, the small γ ($\gamma = 15°$) does not always guarantee a NOT, as shown in Fig. 2(b). The POT unexpectedly emerges in the fringe with the large permittivity, which may be correlated with the emergence of multipoles in high-permittivity materials. Since such high permittivity does not commonly exist in nature, the discussion of this effect is beyond the scope of this Letter. We then keep $\mathrm{Re}(\varepsilon_p) = 16$ and sweep $\mathrm{Im}(\varepsilon_p)$ and a [Fig. 2(c)], showing that the introduction of $\mathrm{Im}(\varepsilon_p)$ diminishes the NOT. This effect can be interpreted by the POT from the absorption, which, for the beam with the LCP propagating along the $-z$ direction, can be given as [20,35,41]

$$\mathbf{M}_{\mathrm{abs}} = \frac{\sigma_{\mathrm{abs}} I_{\mathrm{inc}}}{\omega} \hat{\mathbf{z}}, \tag{3}$$

where σ_{abs} is the absorption cross section, I_{inc} is the incident intensity, and ω is the frequency of light. The triangular prism eventually rotates at a velocity under the balance of optical and fluidic torques [20], which also serves as a paradigm to quantify the optical torque. Other methods include measuring the Stokes parameters [42] or the change of angular momentum of light [43,44], orienting a flat object [45], etc.

To visualize the NOT with the geometry of the TiO_2 triangular prism, the map of the optical torque with the side a and thickness t is depicted in Fig. 3(a). The NOT emerges when the side increases under the illumination of an elliptically polarized beam ($\gamma = 35°$). γ equaling 35° is used instead of 45° (LCP) because that the high permittivity is required to generate the NOT for the LCP [see Fig. 2(a)]. The optical torques on TiO_2 triangular prisms can remain NOTs covering all calculated sizes when $\gamma = 15°$ (see Supplemental Material [38]). Since the optical torque is directly correlated with the distribution of force, we then investigate the energy flow (force) in two prisms ($a = 200$ nm, $t = 150$ nm; $a = 164$ nm, $t = 150$ nm) with opposite optical torques. In the far field, the expression of optical force on a particle can be given as [5,46]

$$\begin{aligned}\mathbf{F} &= -\frac{n}{c}\int_{S_\infty}\{\mathbf{S} - \mathbf{S}^{(i)}\}dS \\ &= -\frac{n}{c}\int_{S_\infty}\{\mathbf{S}^{(\mathrm{mix})} + \mathbf{S}^{(s)}\}dS \\ &= -\frac{n}{8\pi}\int_{S_\infty}\{\mathrm{Re}[\mathbf{E}^{(i)} \times \mathbf{H}^{(s)*} + \mathbf{E}^{(s)} \times \mathbf{H}^{(i)*}] \\ &\quad + \mathrm{Re}[\mathbf{E}^{(s)} \times \mathbf{H}^{(s)*}]\}dS,\end{aligned} \tag{4}$$

where $\mathbf{S}$, $\mathbf{S}^{(i)}$, $\mathbf{S}^{(\mathrm{mix})}$, and $\mathbf{S}^{(s)}$ are the total, incident, mixed, and scattered time-averaged Poynting vectors, respectively; $\mathbf{E}^{(i)}$ and $\mathbf{H}^{(i)}$ denote the incident electric and magnetic fields, respectively. Thus, the optical force can be analyzed by plotting the Poynting vectors. For the normal incidence, $\mathbf{S}^{(s)}$ rotates following the direction of the SAM, while the optical force should be calculated by adding $\mathbf{S}^{(\mathrm{mix})}$, which is shown in Supplemental Material [38]. $\mathbf{S}^{(s)}$ rotates clockwise for the LCP and counterclockwise for the

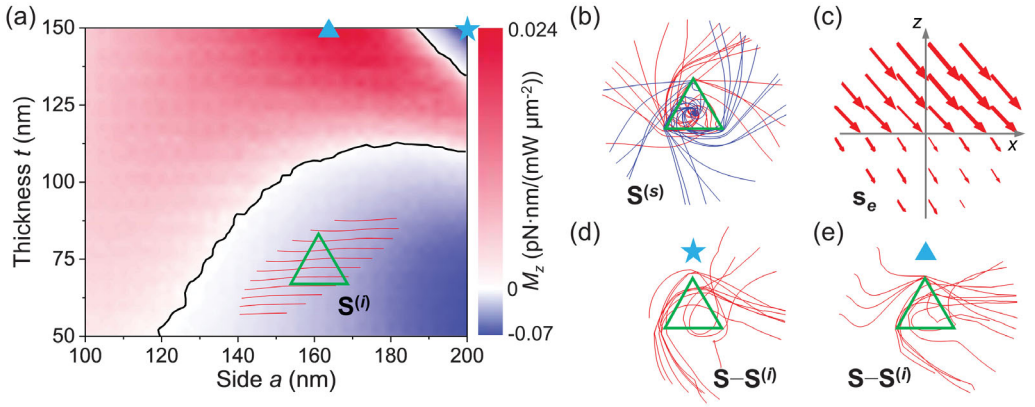

FIG. 3. Size-dependent optical torques on TiO_2 triangular prisms and optical field properties. (a) Optical torque M_z on the TiO_2 ($\varepsilon_p = 2.67^2$) triangular prism versus side a and thickness t in a beam with $\gamma = 35°$ and $\theta = 40°$. M_z on TiO_2 triangular prisms can remain NOTs with different sizes when γ is small (e.g., $\gamma = 15°$, see Supplemental Material [38]). The inset presents the incident Poynting vector in the top view. (b) Stream lines of the scattering Poynting vector $\mathbf{S}^{(s)}$ for the LCP (red lines) and RCP (blue lines) when $\theta = 0$. The clockwise rotation of $\mathbf{S}^{(s)}$ for the LCP and counterclockwise rotation of $\mathbf{S}^{(s)}$ for the RCP rotate the triangular prism counterclockwise and clockwise, respectively, following the direction of the electric SAM $\mathbf{s}_e$. $a = 200$ nm and $t = 150$ nm. (c) Incident SAM for the RCP light with $\theta = 40°$. The SAM is in the same direction as the wave vector. (d) Most of $[\mathbf{S} - \mathbf{S}^{(i)}]$ for the design labeled as the star ($a = 200$ nm, $t = 150$ nm) rotates counterclockwise, meaning that the prism rotates clockwise (NOT). (e) Most of $[\mathbf{S} - \mathbf{S}^{(i)}]$ for the design labeled as the triangle ($a = 164$ nm, $t = 150$ nm) rotate clockwise, meaning that the prism rotates counterclockwise (POT). The rotations of Poynting vectors in (b), (d), and (e) should be seen from the far field (away from the triangular prism).

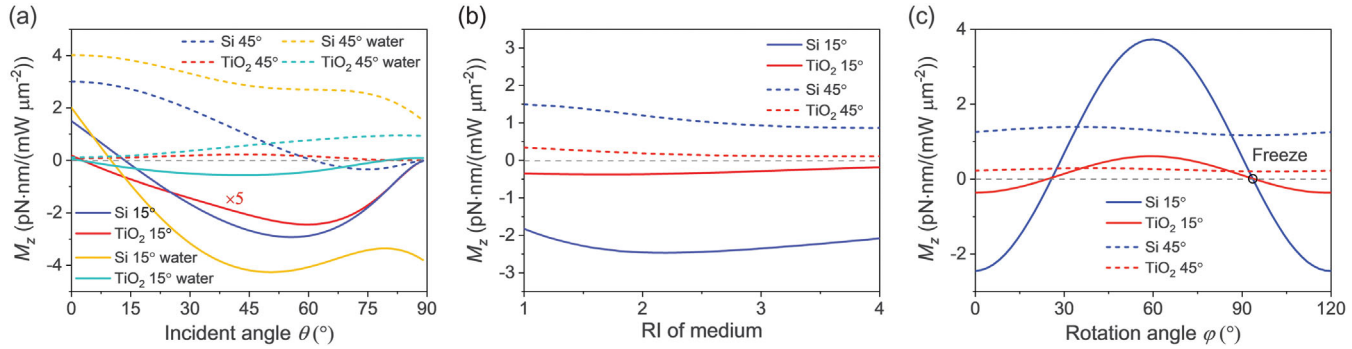

FIG. 4. Control of positive and negative optical torques on triangular prisms made of ordinary materials. (a) Optical torque M_z on the silicon (Si, refractive index $n + ik$, with $n = 4.152$, $k = 0.0518$ at the incident wavelength of 532 nm) and titanium dioxide (TiO_2, $n = 2.67$, $k = 0$) triangular prisms versus the incident angle. "Water" means that the triangular prism ($a = 150$ nm, $t = 150$ nm, rotation angle $\varphi = 0$) is fully immersed in water. The optical torque turns from positive to negative with the increment of the incident angle θ when $\gamma = 15°$. When $\gamma = 45°$ (LCP), the increment of the incident angle also generates NOTs on triangular prisms placed at the interface. Whereas the optical torque remains positive when the triangular prisms are fully immersed in water. (b) The optical torque on the triangular prism ($a = 150$ nm, $t = 150$ nm) does not reverse sign when the refractive index (RI) of the medium increases. (c) Rotation and freeze of the triangular prism versus the rotation angle of triangular prism φ. The optical torques on the Si and TiO_2 triangular prisms keep positive when $\gamma = 45°$. The triangular prism can freeze under the balance of the NOT from $\mathbf{M}_{\text{aniso}}$ and the POT from $\mathbf{M}_{\text{SAM}}$. The incident angles in (b) and (c) are 40°. In (a)–(c), 15° and 45° mean $\gamma = 15°$ and $\gamma = 45°$, respectively.

RCP, representing the counterclockwise and clockwise rotations of the triangular prism, respectively. When the beam is an obliquely incident RCP light wave, the SAM is in the same direction as the wave vector [Fig. 3(c)]. Herein, $\mathbf{S} - \mathbf{S}^{(i)}$ for the design labeled as the star ($a = 200$ nm, $t = 150$ nm) rotates counterclockwise, meaning that the prism rotates clockwise (NOT). Whereas $\mathbf{S} - \mathbf{S}^{(i)}$ for the design labeled as the triangle ($a = 164$ nm, $t = 150$ nm) rotates clockwise, meaning that the prism rotates counterclockwise (POT). Note that the distributions of Poynting vectors should be seen from the far field (away from the triangular prism) as Eq. (4) is applicable in the far field.

By simply changing the incident angles, we can control the rotation directions of the triangular prism, as shown in Fig. 4(a). The POT occurs as expected when $\theta = 0$ (normal incidence) for all configurations. The optical torques, under $\gamma = 15°$, shift from positive to negative when increasing the incident angle. It is also the same situation for the silicon and TiO_2 triangular prims when they are placed at the interface under $\gamma = 45°$ (LCP). Whereas, the optical torque remains positive for triangular prisms fully immersed in water for the LCP. We then plot the curve of the optical torque versus the refractive index of the medium in Fig. 4(b), showing that the sign of optical torque remains unchanged. It is noted that the NOT does not always exist during the rotation of the triangular prism, as shown in Fig. 4(c). This is because that $\mathbf{M}_{\text{aniso}}$ vanishes at the symmetry points (e.g., 30° and 90°), thereby only the positive $\mathbf{M}_{\text{SAM}}$ now occurs. Consequently, the triangular prism freezes at near 90°.

In summary, we have predicted anomalous NOTs emerging from the excitation of obliquely incident light waves with different helicities. S and p polarizations are found to induce the distinct POT and NOT, respectively. The NOT can arise when the orientation angle of the quarter-wave plate $\gamma < 30°$ [Fig. 2(a)], and can also be found in ordinary materials (e.g., TiO_2) for circularly polarized beams with a large incident angle [Fig. 4(a)]. In principle, by exploring the contribution to the NOT from the geometric anisotropy and SAM, we can attribute these abnormal optical torques to the light-matter interaction excited by the in-plane polarization (p polarization) rather than the SAM which induces only the POT.

By changing the incident angles, we can switch the particle rotation direction between clockwise and counterclockwise. We believe that our study not only showcases anomalous optical torques, as illustrated for a triangular prism, but also opens up a new paradigm for polarization-controlled applications in optical forces, light-matter interactions, and physical biology.

Y. S. was Supported by the Fundamental Research Funds for the Central Universities. A. Q. L. acknowledges the Singapore Ministry of Education (MOE) Tier 3 Grant (MOE2017-T3-1-001), Singapore National Research Foundation Grant (MOH-000926), A*STAR research Grant (SERC A18A5b0056) and Singapore's National Water Agency Grant (PUB-1804-0082). T. Z. acknowledges the Natural Science Foundation of China (NSFC), Grant No. 12104083, and Fundamental Research Funds for the Central Universities (DUT22LK27). M. N. V. acknowledges Ministerio de Ciencia, Innovación y Universidades, Grant No. PGC2018-095777-B-C21. D. P. T. acknowledges the support from the UGC/RGC of the Hong Kong Special Administrative Region, China (Project No. AoE/P-502/20), the Department of Science and Technology of Guangdong

Province (2020B1515120073), and Shenzhen Science and Technology Innovation Commission Grant (No. SGDX20190816232811169). P. C. W. acknowledges the support from the Ministry of Science and Technology (MOST), Taiwan (Grants No. 107-2923-M-006-004-MY3; No. 108-2112-M-006-021-MY3; No. 110-2124-M-006-004), and in part from the Higher Education Sprout Project of the Ministry of Education (MOE) to the Headquarters of University Advancement at National Cheng Kung University (NCKU). P. C. W. also acknowledges the support from the Ministry of Education (Yushan Young Scholar Program), Taiwan.

*Corresponding author.
yuzhi_shi01@163.com
†Corresponding author.
eaqliu@ntu.edu.sg
‡Corresponding author.
chengwei.qiu@nus.edu.sg

[1] A. Ashkin, Acceleration and Trapping of Particles by Radiation Pressure, Phys. Rev. Lett. **24**, 156 (1970).
[2] Y. Z. Shi *et al.*, Sculpting nanoparticle dynamics for single-bacteria-level screening and direct binding-efficiency measurement, Nat. Commun. **9**, 815 (2018).
[3] Y. Shi *et al.*, Nanometer-precision linear sorting with synchronized optofluidic dual barriers, Sci. Adv. **4**, eaao0773 (2018).
[4] J. Chen, J. Ng, Z. Lin, and C. T. Chan, Optical pulling force, Nat. Photonics **5**, 531 (2011).
[5] H. Li, Y. Cao, L.-M. Zhou, X. Xu, T. Zhu, Y. Shi, C.-W. Qiu, and W. Ding, Optical pulling forces and their applications, Adv. Opt. Photonics **12**, 288 (2020).
[6] A. Novitsky, C.-W. Qiu, and H. Wang, Single Gradientless Light Beam Drags Particles as Tractor Beams, Phys. Rev. Lett. **107**, 203601 (2011).
[7] Y. Shi *et al.*, Optofluidic microengine in a dynamic flow environment via self-induced back-action, ACS Photonics **7**, 1500 (2020).
[8] Y. Shi, T. Zhu, T. Zhang, A. Mazzulla, D. P. Tsai, W. Ding, A. Q. Liu, G. Cipparrone, J. J. Sáenz, and C.-W. Qiu, Chirality-assisted lateral momentum transfer for bidirectional enantioselective separation, Light Sci. Appl. **9**, 62 (2020).
[9] S. B. Wang and C. T. Chan, Lateral optical force on chiral particles near a surface, Nat. Commun. **5**, 3307 (2014).
[10] F. J. Rodríguez-Fortuño, N. Engheta, A. Martínez, and A. V. Zayats, Lateral forces on circularly polarizable particles near a surface, Nat. Commun. **6**, 8799 (2015).
[11] A. Ashkin, J. M. Dziedzic, J. E. Bjorkholm, and S. Chu, Observation of a single-beam gradient force optical trap for dielectric particles, Opt. Lett. **11**, 288 (1986).
[12] Y. Shi, H. Zhao, L. K. Chin, Y. Zhang, P. H. Yap, W. Ser, C.-W. Qiu, and A. Q. Liu, Optical potential-well array for high-selectivity, massive trapping and sorting at nanoscale, Nano Lett. **20**, 5193 (2020).
[13] D. Haefner, S. Sukhov, and A. Dogariu, Conservative and Nonconservative Torques in Optical Binding, Phys. Rev. Lett. **103**, 173602 (2009).
[14] Y. Shi *et al.*, Nanophotonic array-induced dynamic behavior for label-free shape-selective bacteria sieving, ACS Nano **13**, 12070 (2019).
[15] L. Paterson, M. P. MacDonald, J. Arlt, W. Sibbett, P. E. Bryant, and K. Dholakia, Controlled rotation of optically trapped microscopic particles, Science **292**, 912 (2001).
[16] M. Nieto-Vesperinas, Optical torque on small bi-isotropic particles, Opt. Lett. **40**, 3021 (2015).
[17] L. Tong, V. D. Miljković, and M. Käll, Alignment, rotation, and spinning of single plasmonic nanoparticles and nanowires using polarization dependent optical forces, Nano Lett. **10**, 268 (2010).
[18] K. Y. Bliokh, A. Y. Bekshaev, and F. Nori, Extraordinary momentum and spin in evanescent waves, Nat. Commun. **5**, 3300 (2014).
[19] A. Y. Bekshaev, K. Y. Bliokh, and F. Nori, Transverse Spin and Momentum in Two-Wave Interference, Phys. Rev. X **5**, 011039 (2015).
[20] P. L. Marston and J. H. Crichton, Radiation torque on a sphere caused by a circularly-polarized electromagnetic wave, Phys. Rev. A **30**, 2508 (1984).
[21] S. Chang and S. S. Lee, Optical torque exerted on a homogeneous sphere levitated in the circularly polarized fundamental-mode laser beam, J. Opt. Soc. Am. B **2**, 1853 (1985).
[22] X. Xu and M. Nieto-Vesperinas, Azimuthal Imaginary Poynting Momentum Density, Phys. Rev. Lett. **123**, 233902 (2019).
[23] S. J. Paddack and J. W. Rhee, Rotational bursting of interplanetary dust particles, Geophys. Res. Lett. **2**, 365 (1975).
[24] A. Callegari, M. Mijalkov, A. B. Gököz, and G. Volpe, Computational toolbox for optical tweezers in geometrical optics, J. Opt. Soc. Am. B **32**, B11 (2015).
[25] P. Galajda and P. Ormos, Complex micromachines produced and driven by light, Appl. Phys. Lett. **78**, 249 (2001).
[26] J. Chen, J. Ng, K. Ding, K. H. Fung, Z. Lin, and C. T. Chan, Negative optical torque, Sci. Rep. **4**, 6386 (2014).
[27] N. Sule, Y. Yifat, S. K. Gray, and N. F. Scherer, Rotation and negative torque in electrodynamically bound nanoparticle dimers, Nano Lett. **17**, 6548 (2017).
[28] F. Han, J. A. Parker, Y. Yifat, C. Peterson, S. K. Gray, N. F. Scherer, and Z. Yan, Crossover from positive to negative optical torque in mesoscale optical matter, Nat. Commun. **9**, 4897 (2018).
[29] D. Hakobyan and E. Brasselet, Left-handed optical radiation torque, Nat. Photonics **8**, 610 (2014).
[30] A. Jesacher, S. Fürhapter, C. Maurer, S. Bernet, and M. Ritsch-Marte, Reverse orbiting of microparticles in optical vortices, Opt. Lett. **31**, 2824 (2006).
[31] V. Kajorndejnukul, W. Ding, S. Sukhov, C.-W. Qiu, and A. Dogariu, Linear momentum increase and negative optical forces at dielectric interface, Nat. Photonics **7**, 787 (2013).
[32] T. Zhu, Y. Shi, W. Ding, D. P. Tsai, T. Cao, A. Q. Liu, M. Nieto-Vesperinas, J. J. Sáenz, P. C. Wu, and C.-W. Qiu, Extraordinary Multipole Modes and Ultra-Enhanced Optical Lateral Force by Chirality, Phys. Rev. Lett. **125**, 043901 (2020).

[33] M. Liu, T. Zentgraf, Y. Liu, G. Bartal, and X. Zhang, Light-driven nanoscale plasmonic motors, Nat. Nanotechnol. **5**, 570 (2010).

[34] Y. Shi *et al.*, Superhybrid mode-enhanced optical torques on mie-resonant particles, Nano Lett. **22**, 1769 (2022).

[35] Y. E. Lee, K. H. Fung, D. Jin, and N. X. Fang, Optical torque from enhanced scattering by multipolar plasmonic resonance, Nanophotonics **3**, 343 (2014).

[36] S. Sukhov, V. Kajorndejnukul, R. R. Naraghi, and A. Dogariu, Dynamic consequences of optical spin-orbit interaction, Nat. Photonics **9**, 809 (2015).

[37] I. D. Stoev, B. Seelbinder, E. Erben, N. Maghelli, and M. Kreysing, Highly sensitive force measurements in an optically generated, harmonic hydrodynamic trap, eLight **1**, 7 (2021).

[38] See Supplemental Material at http://link.aps.org/supplemental/10.1103/PhysRevLett.129.053902 for the detailed derivation of the optical torque on a dipole particle as well as Figs. S1–S9.

[39] K. Y. Bliokh and F. Nori, Transverse and longitudinal angular momenta of light, Phys. Rep. **592**, 1 (2015).

[40] M. I. Mishchenko, L. D. Travis, and A. A. Lacis, *Scattering, Absorption, and Emission of Light by Small Particles* (Cambridge University Press, Cambridge, England, 2002).

[41] P. L. Marston, Humblet's angular momentum decomposition applied to radiation torque on metallic spheres using the Hagen-Rubens approximation, J. Quant. Spectrosc. Radiat. Transfer **220**, 97 (2018).

[42] J. H. Crichton and P. L. Marston, The measurable distinction between the spin and orbital angular momenta of electromagnetic radiation, Electron. J. Differ. Equ. **04**, 37 (2000).

[43] F. Strasser, S. M. Barnett, M. Ritsch-Marte, and G. Thalhammer, Generally Applicable Holographic Torque Measurement for Optically Trapped Particles, Phys. Rev. Lett. **128**, 213604 (2022).

[44] A. La Porta and M. D. Wang, Optical Torque Wrench: Angular Trapping, Rotation, and Torque Detection of Quartz Microparticles, Phys. Rev. Lett. **92**, 190801 (2004).

[45] L. Oroszi, P. Galajda, H. Kirei, S. Bottka, and P. Ormos, Direct Measurement of Torque in an Optical Trap and Its Application to Double-Strand DNA, Phys. Rev. Lett. **97**, 058301 (2006).

[46] M. Nieto-Vesperinas, J. J. Sáenz, R. Gómez-Medina, and L. Chantada, Optical forces on small magnetodielectric particles, Opt. Express **18**, 11428 (2010).